SCIENCE CHINA
Chemistry

• ARTICLES •

November 2010 Vol.53 No.11: 2311–2317
doi: 10.1007/s11426-010-4079-8

# Theoretical study of substituent effect on the charge mobility of 2,5-bis(trialkylsilylethynyl)-1,1,3,4-tetraphenylsiloles

ZHAO ZuJin[1], LIU DanDan[2], LAM Jacky Wing Yip[1], LU Ping[2], YANG Bing[2], MA YuGuang[2*] & TANG Ben Zhong[1,3*]

[1]*Department of Chemistry, The Hong Kong University of Science & Technology, Hong Kong, China*
[2]*State Key Laboratory of Supramolecular Structure and Materials; Jilin University, Changchun 130012, China*
[3]*Department of Polymer Science and Engineering, Zhejiang University, Hangzhou 310027, China*

Received May 19, 2010; accepted June 29, 2010

The theoretical calculation of the charge mobility of 2,5-bis(trialkylsilylethynyl)-1,1,3,4-tetraphenylsiloles is presented. B3LYP/6-31* calculations demonstrated that these silole molecules possessed large coupling matrix elements and reorganization energies for electron and hole transfers and high electron mobilities. The bulkiness of the trialkyl substituents influenced the charge mobility of the silole molecules, with the smaller trimethyl group imparting higher charge mobility than triethyl and triisopropyl substituents.

**silole, theoretical calculation, substitution effect, electronic structure, charge mobility**

## 1 Introduction

Siloles (silacyclopentadienes) are silicon-containing five-membered cyclic diens and have attracted extensive attention due to their unique electronic properties and potential high-technological applications. They are considered as novel σ*-π* conjugated materials, in which the σ* orbital of the silicon-carbon bond effectively interacts with the π* orbital of the butadiene fragment, leading to a low-lying lowest unoccupied molecular orbital (LUMO) energy level [1, 2]. As a result, siloles exhibit high electron affinity and fast electron mobility [3]. Recently, great efforts have been made to functionalize siloles and utilize them as electron transport materials [4], light emitters [5–7], building blocks for conducting polymers [8], biosensors [9–11], solar cells [12], etc. Many theoretical studies have been conducted in order to have a better understanding of the substitution effects on their electronic structures and optoelectronic properties [13].

In 2001, we discovered a novel phenomenon of aggregation-induced emission (AIE): A series of propeller-shaped silole molecules are induced to emit efficiently by aggregate formation [14]. The AIE effect greatly boosts their emission efficiency up to unity, turning them from weak fluorophores to strong emitters. This intriguing phenomenon has prompted us to explore more AIE dyes in order to have a better understanding of their structure-property relationship [15–20]. Recently, we have synthesized a group of AIE-active silole derivatives, namely 2,5-bis(trialkylsilylethynyl)-3,4-diphenylsiloles, with varying 1,1- and 2,5-substituents [21]. We investigated their photophysical properties and found that their solid-state emissions are sensitive to the bulkiness of the substituents at the 2,5-positions. Bulky substituents help weaken the intermolecular interactions and restrict the intramolecular rotations, thus imparting the silole molecules with high fluorescence quantum yields. To gain further insight into the substitution effect on the properties of the silole molecules, in this paper we present our theoretical results on the charge mobility of 1,1,3,4-tetraphenylsiloles

*Corresponding author (email: tangbenz@ust.hk; ygma@mail.jlu.edu.cn)

carrying substituents of different bulkiness at the 2,5- positions.

## 2 Experimental

The silole molecules (**1–3**) adopted for the investigation are illustrated in Figure 1, which were prepared according to the procedures published in our previous paper [21]. The crystal structures of the molecules are shown in Figure 2, which were used for the study of the charge mobility and hopping models. The ground-state geometries were optimized using the density functional (DFT) with the B3LYP hybrid functional at the basis set level of 6-31G*, and the unrestricted formalism (UB3LYP) was adopted for the ion-state geometries. All the calculations were performed using Gaussian 03 package in power leader workstation.

## 3 Results and discussion

### 3.1 Electronic structures

We carried out theoretical calculations of **1–3** in order to evaluate the substituent effect on their electronic structures. The torsion angles at the 3,4-positions of the silole ring of **1–3** were almost the same, revealing that the substituents at the 2,5-positions have no pronounced effect on the configurations of the phenyl groups at the 3,4-positions. This may be due to the presence of the triple bond functional bridge groups, which have relieved the steric hindrance between the silole ring and the trialkylsilyl groups.

The highest occupied molecular orbital (HOMO) and LUMO of **1–3** were almost identical (Figure 3). They were mainly dominated by orbitals from the silole ring and the two C≡C triple bonds at the 2,5-postions. The two C≡C triple bonds had significant contributions to both HOMOs and LUMOs because they were arranged almost parallel to the silole ring and hence enjoyed efficient orbital overlapping. The phenyl groups at the 3,4-positons participated and contributed little to the energy levels. Owing to the σ*-π* conjugation, the LUMOs had significant orbital density at

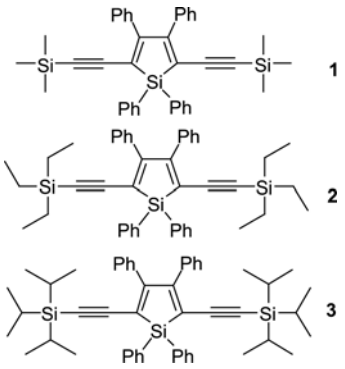


**Figure 1** Molecular structures of 1,1,3,4-tetraphenylsiloles with different 2,5-substituents.

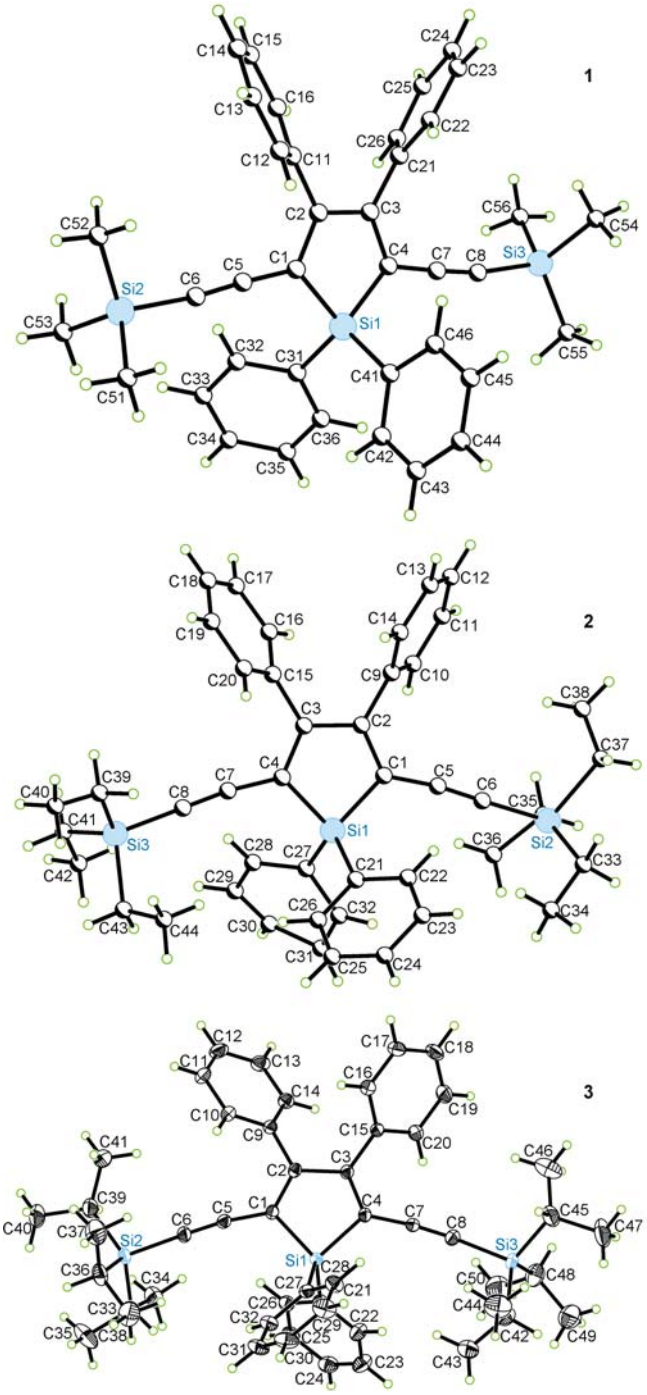


**Figure 2** ORTEP drawings of 1,1,3,4-tetraphenylsiloles (**1–3**).

the two exocyclic Si1–C bonds, which were identical to those of hexaphenylsilole (HPS), methypentaphenylsilole (MPPS), and other silole derivatives [22]. The HOMO and LUMO energy levels of **1** were calculated to be –5.28 and –2.15 eV, respectively, while those of **2** and **3** with larger substituents at the 2,5-positions were located at slightly lower levels of –5.31 and –2.18 eV. The energy band gaps of the silole molecules were the same (3.13 eV) due to their almost identical electronic structures.

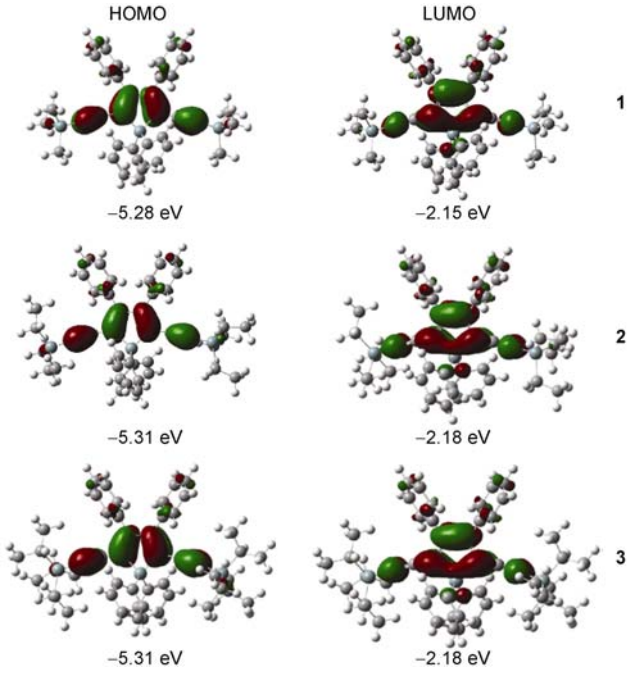


**Figure 3** B3LYP/6-31G* calculated molecular orbital amplitude plots of HOMO and LUMO energy levels of **1–3**.

### 3.2 Cation and anion properties

To investigate whether the substituent can influence the charge mobility of **1–3**, geometry optimizations for both the radical anion and radical cation states (i.e., neutral molecules in the presence of extra electrons and holes) were performed. Figure 4 displays the optimized molecular structures of **1–3** and Table 1 lists the calculated variations of the structural parameters in both states. Similar to HPS, MPPS, and other siloles [22–24], the geometric modifications for **1–3** upon carrier injection were primarily localized within the central portion of the molecular systems, i.e., silole rings with two triple bonds. When an electron was injected (anion), the lengths of the exocyclic Si1–C bonds were increased, while the ring Si1–C bonds became shortened. The *cis*-butadiene portion of the central ring underwent significant decrease in the bond-length alternation as the C–C bonds adjusted to the presence of the extra electron. Meanwhile, the total lengths of the exocyclic C–C single bonds plus the C≡C triple bonds decreased significantly to stabilize the additional charge.

The addition of a hole shortened the exocyclic Si1–C bond but lengthened the ring Si1–C bond. Similar to the anion case, there was a significant change in the bond-length alternation pattern of the C–C bonds in the central ring and the C≡C triple bonds at the 2,5-positions. However, the effect of an additional electron on the lengths of exocyclic Si1–C single and C≡C triple bonds was more profound than that of a hole. With regard to the bond angle, the endocyclic C–Si–C and C–C–Si and exocyclic C–Si–C bond angles changed more significantly in both anion and cation states. The anion had larger endocyclic C–Si–C and smaller exocyclic C–Si–C bond angles than the neutral molecules. The cation exhibited an opposite behavior. The torsion angles of the phenyl groups at the 3,4-positions changed mostly when a hole or electron was injected into the molecules. Both the cation and the anion exhibited smaller torsion angles of the phenyl groups at the 3,4-positions and shorter bridge bond lengths than those of the neutral one, indicating that both the cation and the anion possessed better planarity and higher conjugation. Overall, upon charge injection into **1–3**, geometry relaxation took place mainly in the silole ring and the adjacent C≡C triple bonds at the 2,5-positions. The conformations of the trialkyl groups changed little in the anion and cation compared with those in the neutral state.

### 3.3 Reorganization energy and charge mobility

After studying the cation and anion properties of **1–3**, we

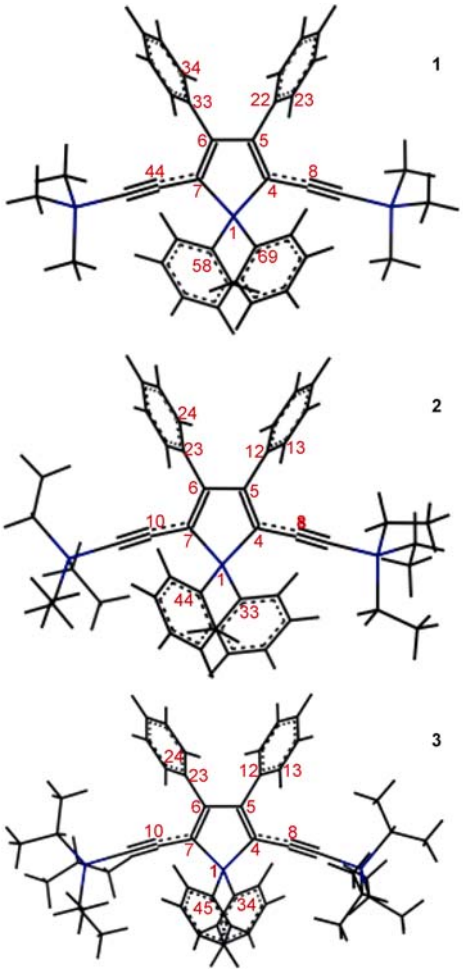


**Figure 4** Optimized molecular structures of **1–3**.

**Table 1** Calculated variations of structural parameters in the anion and cation for **1–3** [a)]

| **1** | | | **2** | | | **3** | | |
|---|---|---|---|---|---|---|---|---|
| | anion | cation | | anion | cation | | anion | cation |
| | | | bond length (Å) | | | | | |
| R(1,4) | –0.026 | 0.016 | R(1,4) | –0.025 | 0.016 | R(1,4) | –0.025 | 0.015 |
| R(1,7) | –0.026 | 0.016 | R(1,7) | –0.026 | 0.015 | R(1,7) | –0.025 | 0.015 |
| R(1,58) | 0.022 | –0.014 | R(1,33) | 0.022 | –0.014 | R(1,34) | 0.021 | –0.013 |
| R(1,69) | 0.022 | –0.014 | R(1,44) | 0.021 | –0.013 | R(1,45) | 0.021 | –0.013 |
| R(4,5) | 0.048 | 0.038 | R(4,5) | 0.048 | 0.038 | R(4,5) | 0.048 | 0.038 |
| R(4,8) | –0.015 | –0.023 | R(4,8) | –0.015 | –0.023 | R(4,8) | –0.015 | –0.024 |
| R(5,6) | –0.057 | –0.042 | R(5,6) | –0.057 | –0.042 | R(5,6) | –0.057 | –0.042 |
| R(5,22) | –0.003 | –0.010 | R(5,12) | –0.003 | –0.009 | R(5,12) | –0.003 | –0.009 |
| R(6,7) | 0.048 | 0.038 | R(6,7) | 0.048 | 0.038 | R(6,7) | 0.048 | 0.038 |
| R(6,33) | –0.003 | –0.010 | R(6,23) | –0.003 | –0.010 | R(6,23) | –0.003 | –0.009 |
| R(7,44) | –0.015 | –0.023 | R(7,10) | –0.015 | –0.024 | R(7,10) | –0.015 | –0.024 |
| | | | bond angle (°) | | | | | |
| A(1,4,5) | –0.9 | 2.0 | A(1,4,5) | –0.8 | 1.9 | A(1,4,5) | –0.8 | 1.9 |
| A(4,5,6) | 0.2 | –0.7 | A(4,5,6) | 0.2 | –0.6 | A(4,5,6) | 0.2 | –0.6 |
| A(5,6,7) | 0.2 | –0.7 | A(5,6,7) | 0.2 | –0.8 | A(5,6,7) | 0.2 | –0.6 |
| A(6,7,1) | –0.9 | 2.0 | A(6,7,1) | –0.8 | 2.1 | A(1,7,6) | –0.8 | 1.9 |
| A(7,1,4) | 1.3 | –2.6 | A(7,1,4) | 1.3 | –2.6 | A(4,1,7) | 1.3 | –2.5 |
| A(58,1,69) | –4.8 | 3.3 | A(44,1,33) | –4.6 | 3.2 | A(34,1,45) | –4.3 | 3.0 |
| | | | torsion angle (°) | | | | | |
| D(8,4,5,6) | 1.6 | 0.9 | D(8,4,5,6) | –1.4 | 0.6 | D(8,4,5,6) | –1.5 | –0.8 |
| D(23,22,5,6) | –4.1 | –2.4 | D(13,12,5,6) | 4.2 | 2.7 | D(6,5,12,13) | 4.0 | 2.8 |
| D(34,33,6,7) | –2.6 | –1.6 | D(24,23,6,7) | 2.6 | 2.3 | D(7,6,23,24) | 2.7 | 1.8 |
| D(44,7,6,5) | 1.9 | 0.8 | D(10,7,6,5) | –2.3 | –1.6 | D(5,6,7,10) | –2.3 | –0.8 |
| D(4,5,6,7) | –1.1 | –1.7 | D(4,5,6,7) | 0.9 | 1.4 | D(4,5,6,7) | 1.0 | 1.5 |
| D(1,4,5,6) | 0.7 | 1.2 | D(1,4,5,6) | –0.4 | –0.6 | D(1,4,5,6) | –0.7 | –1.2 |

a) Abbreviations: R = bond length, A = bond angle, D = torsion angle.

then calculated the barriers for electron and hole transfer in the radical anion and radical cation species, and the charge mobility of **1–3**. To describe the charge transport in the crystal state, we considered an incoherent hopping model, in which the charge can only transfer between adjacent molecules. Viewing each hopping event as a nonadiabatic electron transfer reaction, we used standard Marcus theory [25, 26] to express the rate of charge motion between neighboring molecules, $W$, in terms of the reorganization energy ($\lambda$) and the coupling matrix element ($V$). Assuming that the temperature is sufficiently high that vibrational modes can be treated classically, we obtained eq. (1):

$$W = \frac{V^2}{\hbar}\left(\frac{\pi}{\lambda k_B T}\right)^{1/2} \exp\left(-\frac{\lambda}{4k_B T}\right) \tag{1}$$

where $k_B$ is the Boltzmann constant and $T$ is the temperature (298 K). Given the hopping rate between two neighbors, the diffusion coefficient can be evaluated as eq. (2):

$$D = \frac{1}{2n}\sum_i r^2 W_i P_i \tag{2}$$

where $n$ is the dimensionality, $W_i$ is the hopping rate due to the charge carrier to the ith neighbor, $r$ is the distance to neighbor $i$, and $P_i$ is the relative probability for the charge carrier to a particular $i$th neighbor and is expressed by eq. (3).

$$P_i = W_i \Big/ \sum_i W_i \tag{3}$$

In eq. (2), $2n = 6$ leads to the diffusion coefficient in a special direction, while $2n = 6$ summing overall possible hops leads to the averaged diffusion coefficient. The drift mobility of hopping, $\mu$, is then evaluated from the Einstein relation,

$$\mu = \frac{e}{k_B T} D \tag{4}$$

where $e$ is the electronic charge.

Only when the intermolecular transfer integral ($V$) and the reorganization energy ($\lambda$) have been calculated in advance can the average drift mobility be evaluated using eqs. (1)–(4).

A direct dimer hamiltonian method was adopted to calculate the intermolecular transfer integral ($V$). It can be written as eq. (5):

$$V_{+/-} = \left\langle \phi_{HOMO/LUMO}^{0,\text{site1}} \middle| F^0 \middle| \phi_{HOMO/LUMO}^{0,\text{site2}} \right\rangle \quad (5)$$

where $\left\langle \phi_{HOMO/LUMO}^{0,\text{site1}} \right|$ and $\left| \phi_{HOMO/LUMO}^{0,\text{site2}} \right\rangle$ represents the HOMO/LUMO wave functions of two isolated molecules' sites 1 and 2, respectively. $F^0$ is the Fock matrix constructed from the density matrix of the noninteracting dimer, which can be evaluated as $F = SC\varepsilon C^{-1}$, where $S$ is the overlap matrix of the dimer, and the Kohn-Sham orbital coefficient $C$ and energy eigenvalue $\varepsilon$ are obtained by one-step diagonalization without iteration.

The reorganization energy ($\lambda$) can be separated into the sum of two primary components: (i) the medium reorganization energy that arises from modifications to the polarization of the surrounding medium due to the presence of excess charges ($\lambda_s$) and (ii) the intramolecular reorganization energy ($\lambda_i$), which corresponds to the sum of geometry relaxation energies upon going from the neutral-state geometry to the charged-state geometry and vice versa. Hence, $\lambda$ for hole and electron transfer is given by eq. (6):

$$\lambda_{+/-} = \left(E_{ng}^{+/-} - E_{cg}^{+/-}\right) + \left(E_{cg} - E_{ng}\right) \quad (6)$$

Here, $E_{ng}^{+/-}$ and $E_{ng}$ are the energies of the charged-state and neutral-state with the neutral-state geometry, respectively; $E_{cg}^{+/-}$ and $E_{cg}$ are the energies of the charged-state and neutral-state with the charged-state geometry, respectively. Considering the negligible medium reorganization energy in the solid state, we calculated the intramolecular contribution to the total reorganization energies for electron and hole transfer, separately, and the results are compared in Table 2. The charge-hopping pathways for each molecule were calculated based on their crystal structures as illustrated in Figure 5.

The calculation results show 10 charge-hopping pathways for **1**, and 8 and 5 for **2** and **3**, respectively. The maximum coupling matrix element (V) for electron transfer of **1**, which might give the most significant contribution to the average electron mobility, was $1.52 \times 10^{-3}$ eV. This value was much higher than those of **2** ($0.91 \times 10^{-3}$ eV) and **3** ($0.88 \times 10^{-3}$ eV). The similar decrease of maxima V values with the increase of substituent sizes was observed for the hole transfer of **1–3**. The total reorganization energy for electron transfer ($\lambda_-$) of **1** was 0.505 eV, which was higher than those of **2** (0.488 eV) and **3** (0.490 eV). The similar trend was observed from their total reorganization energies for hole transfer ($\lambda_+$). The $\lambda_-$ energies of **1–3** were quite close to those of HPS (0.49 eV) and other pyridine-substituted siloles (~0.50 eV) [23]. From the calculated total reorganization energies, the charge transfer activation energies could be evaluated to be ~0.1 eV, a clear indicator being dynamically favorable to the charge transfer of these silole molecules. These results show that the charge mobility sensitively depends on the coupling matrix elements.

The electron mobility of **1**, **2**, and **3** was calculated to be $1.33 \times 10^{-5}$, $7.25 \times 10^{-6}$, and $4.06 \times 10^{-6}$ cm$^2$ V$^{-1}$ s$^{-1}$,

**Table 2** Calculated transport characteristics of **1–3**

| | | | | | | | | | | | |
|---|---|---|---|---|---|---|---|---|---|---|---|
| **1** | Pathway | 1 | 2 | 3 | 4 | 5 | 6 | 7 | 8 | 9 | 10 |
| | Distance (Å) | 11.97 | 9.96 | 10.39 | 7.96 | 8.23 | 10.52 | 9.43 | 10.62 | 12.04 | 9.43 |
| | $V_+$ (meV) | 0.0513 | 0.00354 | 0.0358 | 0.60 | 0.50 | 0.39 | 0.0360 | 0.90 | 0.0001 | 0.036 |
| | $V_-$ (meV) | 0.19 | 0.00392 | 0.0977 | 0.63 | 1.52 | 0.76 | 0.19 | 0.00642 | 0.0311 | 0.19 |
| | $\lambda$ (eV) | | 0.414 ($\lambda_+$) | | 0.505 ($\lambda_-$) | | | | | | |
| | Mobility $\mu$ (cm$^2$ V$^{-1}$ s$^{-1}$) | | $1.67 \times 10^{-5}$ ($\mu_+$) | | $1.33 \times 10^{-5}$ ($\mu_-$) | | | | | | |
| **2** | Pathway | 1 | 2 | 3 | 4 | 5 | 6 | 7 | 8 | | |
| | Distance (Å) | 7.53 | 10.81 | 9.16 | 6.52 | 13.06 | 12.89 | 14.29 | 14.29 | | |
| | $V_+$ (meV) | 0.13 | 0.0478 | 0.017 | 0.26 | 0 | 0.00001 | 0.0482 | 0.0482 | | |
| | $V_-$ (meV) | 0.68 | 0.0418 | 0.91 | 0.0781 | 0.00004 | 0.00003 | 0.00394 | 0.00394 | | |
| | $\lambda$ (eV) | | 0.405 ($\lambda_+$) | | 0.488 ($\lambda_-$) | | | | | | |
| | Mobility $\mu$ (cm$^2$ V$^{-1}$ s$^{-1}$) | | $7.35 \times 10^{-7}$ ($\mu_+$) | | $7.25 \times 10^{-6}$ ($\mu_-$) | | | | | | |
| **3** | Pathway | 1 | 2 | 3 | 4 | 5 | | | | | |
| | Distance (Å) | 6.68 | 11.09 | 13.13 | 7.52 | 15.63 | | | | | |
| | $V_+$ (meV) | 0.22 | 0.0593 | 0 | 0.0753 | 0.0352 | | | | | |
| | $V_-$ (meV) | 0.88 | 0.25 | 0.00005 | 0.71 | 0.017 | | | | | |
| | $\lambda$ (eV) | | 0.393 ($\lambda_+$) | | 0.490 ($\lambda_-$) | | | | | | |
| | Mobility $\mu$ (cm$^2$ V$^{-1}$ s$^{-1}$) | | $6.94 \times 10^{-7}$ ($\mu_+$) | | $4.06 \times 10^{-6}$ ($\mu_-$) | | | | | | |

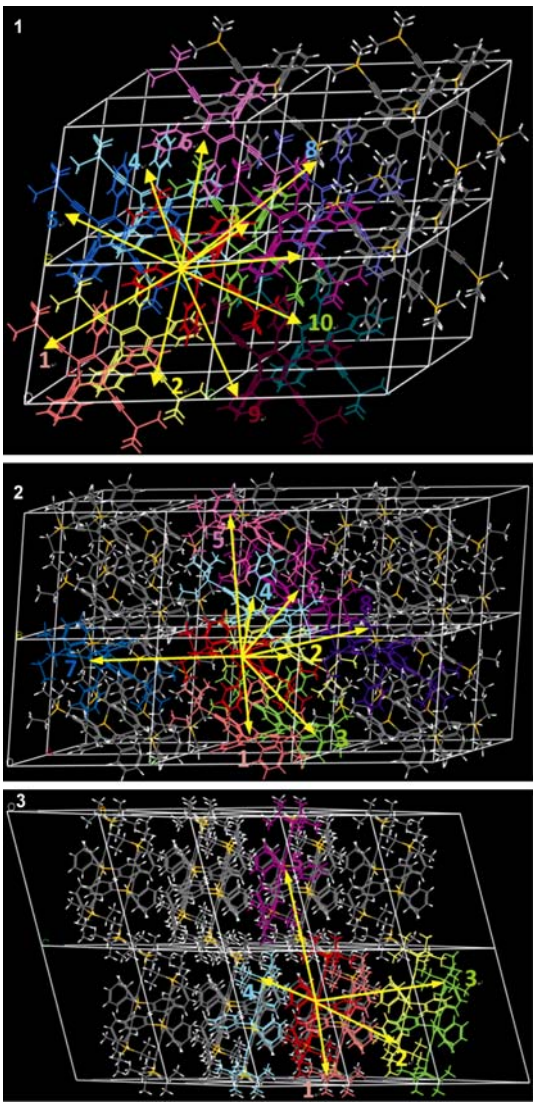

**Figure 5** Hopping pathways for molecules **1**–**3** from their corresponding crystal structures.

respectively. The hole mobility of the silole molecules also decreased with an increase in the substituent volume. The higher charge mobility of **1** is attributed to its smallest trimethyl substituents, which enable a more compact stacking of molecules. This shortens the intermolecular distances and encourages larger coupling matrix elements and higher charge-hopping rates.

## 4 Conclusions

In this work, we investigated the substituent effect on the charge mobility of 1,1,3,4-tetraphenylsiloles with 2,5-substituents by theoretical calculations. The geometric modifications that occurred during the reduction and oxidation of the silole molecules were primarily localized at the silole ring, two C≡C triple bonds, and the exocyclic Si1–C bonds. Whereas the non-conjugated trialkyl substituents had little influence on the electronic structures of the silole molecules, the sizes of the substituents significantly affected the coupling matrix elements and thus the charge mobility. While **1** with small trimethyl substituents exhibited the largest reorganization energies, coupling matrix elements and the highest charge mobility, **3** showed opposite behaviors because its bulky triisopropyl substituents have effectively hampered the close packing of the molecules and hence decreased the hopping rate between the central conjugated silole rings. These results may provide useful information for the understanding of the conductivity and structure-property relationship of this kind of silole molecules.

*This work was supported by the Research Grants Council of Hong Kong (602707, 601608, ITP/008/09NP and 603505), the National Natural Science Foundation of China (20634020) and the Ministry of Science and Technology of China (2002CD613401). TANG Ben Zhong thanks the support from the CAO GuangBiao Foundation of Zhejiang University.*

1 Khabashesku VN, Balaji V, Boganov SE, Nefedov OM, Michl J. Matrix isolation of silacyclopentadienes: UV-visible and IR spectra and photochemical interconversion. *J Am Chem Soc*, 1994, 116: 320–329
2 Yamaguchi S, Tamao K. Silole-containing σ- and π-conjugated compounds. *J Chem Soc Dalton Trans*, 1998, 3693–3702
3 Mäkinen AJ, Uchida M, Kafafi ZH. Electronic structure of a silole derivative-magnesium thin film interface. *J Appl Phys*, 2004, 95: 2832–2838
4 Murata H, Kafafi ZH, Uchida M. Efficient organic light-emitting diodes with undoped active layers based on silole derivatives *Appl Phys Lett*, 2002, 80: 189–191
5 Tang BZ, Zhan X, Yu G, Lee PPS, Liu Y, Zhu D. Efficient blue emission from siloles. *J Mater Chem*, 2001, 11: 2974–2978
6 Zhao Z, Chen S, Lam JWY, Jim CKW, Chan CYK, Wang Z, Lu P, Kwok HS, Ma Y, Tang BZ. Steric hindrance, electronic communication, and energy transfer in the photo- and electroluminescence processes of aggregation-induced emission luminogens. *J Phys Chem C*, 2010, 114: 7963–7972
7 Chen HY, Lam JW, Luo JD, Ho YL, Tang BZ, Zhu D, Wong M, Kwok HS. Highly efficient organic light-emitting diodes with a silole-based compound. *Appl Phys Lett*, 2002, 81: 574–576
8 Usta H, Lu G, Facchetti A, Marks TJ. Dithienosilole- and dibenzosilole-thiophene copolymers as semiconductors for organic thin-film transistors. *J Am Chem Soc*, 2006, 128: 9034–9035
9 Dong YQ, Lam JWY, Qin AJ, Li Z, Liu JZ, Sun JZ, Dong YP, Tang BZ. Endowing hexaphenylsilole with chemical sensory and biological probing properties by attaching amino pendants to the silolyl core. *Chem Phys Lett*, 2007, 446: 124–127
10 Peng L, Wang M, Zhang G, Zhang D, Zhu D. A fluorescence turn-on detection of cyanide in aqueous solution based on the aggregation-induced emission. *Org Lett*, 2009, 11: 1943–1946
11 Yu Y, Hong Y, Feng C, Liu J, Lam JWY, Faisal M, Ng KM, Luo KQ, Tang BZ. Synthesis of an AIE-active fluorogen and its application in cell imaging. *Sci Chin Ser B Chem*, 2009, 52: 15–19
12 Mi B, Dong Y, Li Z, Lam JWY, Häußler M, Sung HHY, Kwok HS, Dong Y, Williams ID, Liu Y, Luo Y, Shuai Z, Zhu D, Tang BZ. Making silole photovoltaically active by attaching carbazolyl donor groups to the silolyl acceptor core. *Chem Commun*, 2005, 3583–3585
13 Yamaguchi S, Endo T, Uchida M, Izumizawa T, Furukawa K, Tamao K. Toward new materials for organic electroluminescent devices: synthesis, structures, and properties of a series of 2,5-diaryl-3,4-diphenylsiloles. *Chem Eur J*, 2000, 6: 1683–1692

14 Luo JD, Xie ZL, Lam JWY, Cheng L, Chen HY, Qiu CF, Kwok HS, Zhan XW, Liu YQ, Zhu DB, Tang BZ. Aggregation-induced emission of 1-methyl-1,2,3,4,5-pentaphenylsilole. *Chem Commun*, 2001, 1740–1741
15 Zhao Z, Chen S, Shen X, Mahtab F, Yu Y, Lu P, Lam JWY, Kwok HS, Tang BZ. Aggregation-induced emission, self-assembly, and electroluminescence of 4,4′-bis(1,2,2-triphenylvinyl)biphenyl. *Chem Commun*, 2010, 46: 686–688
16 Hong Y, Lam JWY, Tang BZ. Aggregation-induced emission: Phenomenon, mechanism and applications. *Chem Commun*, 2009, 4332–4353
17 Liu J, Lam JWY, Tang BZ. Aggregation-induced emission of silole molecules and polymers: Fundamental and applications. *J Inorg Organomet Polym*, 2009, 19: 249–285
18 Zhao Z, Chen S, Lam JWY, Chan CYK, Jim CKW, Wang Z, Wang C, Lu P, Kwok HS, Ma Y, Tang BZ. Luminescent tetraphenylethene-substituted silanes. *Pure Appl Chem*, 2010, 82: 863–870
19 Li Z, Dong Y, Lam JWY, Sun J, Qin A, Häußler M, Dong Y, Sung HHY, Williams ID, Kwok HS, Tang BZ. Functionalized siloles: Versatile synthesis, aggregation-induced emission, and sensory and device applications. *Adv Funct* Mater. 2009, 19: 1–13
20 Zhao Z, Chen S, Lam JWY, Lu P, Zhong Y, Wong K, Kwok HS, Tang BZ. Creation of highly efficient solid emitter by decorating pyrene core with AIE-active tetraphenylethene peripheries. *Chem Commun*, 2010, 46: 2221–2223
21 Zhao Z, Wang Z, Lu P, Chan CYK, Liu D, Lam JWY, Sung HHY, Williams ID, Ma Y, Tang BZ. Structural modulation of solid-state emission of 2,5-bis(trialkylsilylethynyl)-3,4-diphenylsiloles. *Angew Chem Int Ed*, 2009, 48: 7608–7611
22 Yu G, Yin SW, Liu YQ, Chen JS, Xu XJ, Sun XB, Ma DG, Zhan XW, Peng Q, Shuai ZG, Tang BZ, Zhu DB, Fang WH, Luo Y. Structures, electronic states, photoluminescence, and carrier transport properties of 1,1-disubstituted 2,3,4,5-tetraphenylsiloles. *J Am Chem Soc*, 2005, 127: 6335–6346
23 Risko C, Kushto G P, Kafafi Z H, Brédas J L. Electronic properties of silole-based organic semiconductors. *J Chem Phys*, 2004, 121: 9031–9038
24 Zhan X, Risko C, Korlyukov A, Sena F, Timofeeva TV, Antipin MY, Barlow S, Brédas JL, Marder SR. Comparative studies of the geometric and electronic properties of 1,1-disubstituted-2,3,4,5-tetraphenylsiloles and 1,1,2,2-tetramethyl-3,4,5,6-tetraphenyl-1,2-disila-3,5-cyclohexadiene. *J Mater Chem*, 2006, 16: 3814–3822
25 Marcus R A. Electron transfer reactions in chemistry. Theory and experiment. *Rev Mod Phys*, 993, 65: 599–610
26 Marcus RA, Eyring H. Chemical and electrochemical electron-transfer theory. *Annu Rev Phys Chem*, 1964, 15: 155–196